

Hemodynamic forces can be accurately measured in vivo with optical tweezers

Sébastien Harlepp^{a,b,c,*}, Fabrice Thalmann^{a,d}, Gautier Follain^{a,e,f,g}, and Jacky G. Goetz^{a,e,f,g,*}

^aUniversité de Strasbourg, 67000 Strasbourg, France; ^bIPCMS, UMR7504, 67200 Strasbourg, France; ^cLabEx NIE and ^fLabEx Medalis, Université de Strasbourg, 67000 Strasbourg, France; ^dICS, UPR22, 67034 Strasbourg, France; ^eInserm UMR_S1109, MN3T, 67200 Strasbourg, France; ^gFédération de Médecine Translationnelle de Strasbourg (FMTS), 67000 Strasbourg, France

ABSTRACT Force sensing and generation at the tissue and cellular scale is central to many biological events. There is a growing interest in modern cell biology for methods enabling force measurements in vivo. Optical trapping allows noninvasive probing of piconewton forces and thus emerged as a promising mean for assessing biomechanics in vivo. Nevertheless, the main obstacles lie in the accurate determination of the trap stiffness in heterogeneous living organisms, at any position where the trap is used. A proper calibration of the trap stiffness is thus required for performing accurate and reliable force measurements in vivo. Here we introduce a method that overcomes these difficulties by accurately measuring hemodynamic profiles in order to calibrate the trap stiffness. Doing so, and using numerical methods to assess the accuracy of the experimental data, we measured flow profiles and drag forces imposed to trapped red blood cells of living zebrafish embryos. Using treatments enabling blood flow tuning, we demonstrated that such a method is powerful in measuring hemodynamic forces in vivo with accuracy and confidence. Altogether this study demonstrates the power of optical tweezing in measuring low range hemodynamic forces in vivo and offers an unprecedented tool in both cell and developmental biology.

Monitoring Editor

Manuel Théry
CEA, Hopital Saint Louis

Received: Jun 15, 2017

Revised: Sep 5, 2017

Accepted: Sep 6, 2017

INTRODUCTION

Integration of biomechanics in cell biology studies has grown exponentially in the past few years. The early observation that mechanical signals drive and modulate signaling pathways within cells through mechano-transduction has led to a paradigm shift when approaching cell biological phenomena. Developmental biologists have led the way and undertook a series of mechanical manipulations and measurements to grasp the interplay between biomechanics and tissue morphogenesis (Petridou *et al.*, 2017).

Accurate manipulation, measurement, and quantification of tissue and cellular forces in vivo are essential to such task. There are several research fields where quantification of forces in vivo is central. For example, the progression of many diseases such as cancer, cardiomyopathies, and myopathies is tightly linked to biomechanics. Much attention has been given to the interplay between static forces such as tissue elasticity and tumor progression (Jain *et al.*, 2014). However, the biological ramifications of fluid forces, in development (Freund *et al.*, 2012) and disease progression (Provenzano and Hingorani, 2013), are obvious, and methods are needed for fine probing of these forces in vivo. Metastatic extravasation of circulating tumor cells (CTCs) is strongly influenced by mechanical inputs such as shear and adhesion forces, as well as vascular architecture (Wirtz *et al.*, 2011; Azevedo *et al.*, 2015). Similar to the extravasation of immune cells in an inflammatory context, efficient adhesion of CTCs to the vascular wall is needed before engaging in extravasation (Reymond *et al.*, 2013). While experiments have been largely performed in vitro (Chang *et al.*, 2016; Labernadie *et al.*, 2017), there is a growing need for establishing similar approaches in vivo enabling high-accuracy measurements of forces in realistic physio-pathological situations.

This article was published online ahead of print in MBoC in Press (<http://www.molbiolcell.org/cgi/doi/10.1091/mbc.E17-06-0382>) on September 13, 2017.

*Address correspondence to: Sébastien Harlepp (harlepp@unistra.fr) or Jacky G. Goetz (jacky.goetz@inserm.fr; www.goetzlab.com, twitter: @GoetzJacky).

© 2017 Harlepp *et al.* This article is distributed by The American Society for Cell Biology under license from the author(s). Two months after publication it is available to the public under an Attribution–Noncommercial–Share Alike 3.0 Unported Creative Commons License (<http://creativecommons.org/licenses/by-nc-sa/3.0>).

Abbreviations used: AFM, atomic force microscopy; CTC, circulating tumor cell; DA, dorsal aorta; dpf, days postfertilization; ISV, intersegmental vein; OT, optical tweezers; PIV, particle image velocimetry; RBC, red blood cell; ZF, zebrafish.

"ASCB®," "The American Society for Cell Biology®," and "Molecular Biology of the Cell®" are registered trademarks of The American Society for Cell Biology.

However, performing such experiments *in vivo* needs to overcome two major hurdles: it should be noninvasive and also should be able to reach deep tissues. Such limitations prevent the use of several contact techniques such as atomic force microscopy (AFM), but led to the development of noninvasive and noncontact tools such as magnetic tweezers (Desprat *et al.*, 2008; Brunet *et al.*, 2013) or optical tweezers (OT) (Ashkin and Dziedzic, 1987; Hörner *et al.*, 2017).

Optical tweezers suffer from the inconvenience of calibration *in vivo* and from limitation in the application in deep tissues. While trapping cells *in vivo*, one needs to calibrate the setup for every single cell that is trapped. Indeed, heterogeneity of cell size and of the refractive index prevents us from applying a single calibration to multiple situation. Nevertheless, OT permit a dynamic analysis of the mechanical properties of cells (Huang *et al.*, 2003; Monachino *et al.*, 2017) and tissues (Lopez-Quesada *et al.*, 2014; Gao *et al.*, 2016) without altering embryonic development. Optical tweezing thus offers a wide palette for trapping and potentially measuring fluid forces *in vivo*. Recent pioneer work has shown that red blood cells (RBCs) can be trapped using optical tweezing in capillary vessels from mouse ears (Zhong *et al.*, 2013). In this study, the authors moved the trapped RBC through the capillary vessel and thereby induced artificial clots in the circulation. Although very powerful and promising, such a technique remains limited when studying events located deep in tissues.

The recent emergence of the zebrafish (ZF) embryo allows, due to its relative optical transparency, the use of a wide plethora of optical tools. Taking advantage of that property, Johansen *et al.* (2016) recently demonstrated the power of optical tweezing in a living ZF embryo. They trapped and displaced multiple cell types in the blood flow, such as RBCs or macrophages and brought these cell types in contact with the vascular wall. Although this interesting study shows a large panel of potential applications, it does not provide an accurate quantification of the range of forces exerted or applied on the different objects. A few years earlier, we used a similar approach for quantifying the importance of the viscoelasticity of the arterial walls in ZF embryos by trapping RBCs at different positions of the vasculature (Anton *et al.*, 2013). To our knowledge, this study was the first providing quantitative values from optical tweezing *in vivo*. We further used this approach to address the adhesion of epicardial cells to the pericardium during cardiac development in the ZF embryo (Peralta *et al.*, 2013). More recently, oscillating OT deforming cell junctions on the *Drosophila* embryo (Bambardekar *et al.*, 2015; Sugimura *et al.*, 2016) allowed the authors to accurately measure the tension forces between adjacent cells around 44pN.

Nevertheless, all these studies face a major obstacle, that is, the calibration of the optical trap, which limits the use of OT in realistic *in vivo* contexts. Recently calibration of OT *in situ* has been achieved (Staunton *et al.*, 2017). We provide here a mean to achieve accurate calibration in the context of probing hemodynamic forces in the ZF embryo. We first describe how to reach and quantify the physical parameters of the system by using high-speed imaging methods combined with image processing. Then we describe how trapping of RBCs at different positions in the vasculature is processed in order to quantify the trap stiffness and to calculate the associated forces. We provide a numerical approach allowing us to solve the differential equation of the movement and compare the numerical data with the experimental ones to confirm the power of such calibration. Finally, we validate our approach by tuning heart pacemaker activity and by measuring its impact on hemodynamic forces.

RESULTS AND DISCUSSION

Fine measurement of velocity profiles for calibration of optical tweezers *in vivo*

Accurate calibration of OT *in vivo* requires a fine assessment of the physical parameters over time and space. Here we introduce a method for accurate measurements of hemodynamic profiles in the ZF embryo. Hemodynamic profiles are measurements of velocity as a function of time, at a clearly located position in the ZF embryo. Such a method could be very useful in understanding the role played by hemodynamic forces in vascular morphogenesis, and also in pathological scenarios such as intravascular arrest and extravasation of CTCs or immune cells. We focused our analysis on the caudal plexus region of the ZF embryo (Figure 1A), whose optical characteristics and relative three-dimensional (3D) structure make it optimal for high-speed imaging of the blood flow. We first perform high-speed imaging of the blood flow, at 200 frames per second (fps) and at intermediate magnification. Such a frame rate is optimal for fine tracking individual RBCs in the vasculature (Supplemental Movie S1). Raw acquisitions are processed to enhance the contrast of RBCs in the blood flow (Figure 1B and Supplemental Movie S1). Subsequently the processed data set is analyzed through a PIV (particle imaging velocimetry) plug-in developed on ImageJ that is well-suited for automatic analysis of the blood flow movie (Figure 1B and Supplemental Movie S1). The PIV allows a fine measurement of the velocity amplitudes and profiles at any position within the vasculature at a given time. Such a step is of utmost importance while studying hemodynamics with a Poiseuille-type distribution where velocity profiles vary significantly along a cross-section of a single vessel (Figure 1B). However, PIV analysis requires several parameters to be adjusted manually. While these parameters can potentially influence the measured velocities, we undertook a parallel approach aiming to extract the flow profiles of several RBCs using manual tracking performed in Fiji and rendered using Imaris software (Figure 1C and Supplemental Movie S2). Because most of the RBCs follow the central streamline (Amini *et al.*, 2014), manual tracking of individual RBCs allows us to determine the flow profiles in the center of the measured vessel. We then compare these profiles to the ones obtained upon PIV treatment. The comparison of the two methods allows us to estimate the accuracy of our measurements, which is around 50 $\mu\text{m/s}$ for the determination of the blood flow velocity. We then fitted the PIV experimental curves with theoretical profiles (Figure 1C). The function used is adapted from our previous work (Anton *et al.*, 2013) and can be written as follows:

$$v(t) = \left(v_{\max} * \text{abs} \left(\tanh \left(3 * \sin \left(\pi * (f * t - \varphi) \right) \right) - \tanh \left(3 * \sin \left(\pi * (f * t - \varphi) - (\pi / 4) \right) * e^{(-\tau)} \right) \right) \right) + v_0$$

where v_{\max} represents the maximal velocity, f the heart beat frequency, φ the phase shift representing the arbitrary origin of the experimental signal, v_0 the minimal velocity, and τ the damping during the diastolic phase linked to the endothelial barrier viscoelastic behavior.

Combining these different methods allows for a very accurate assessment of velocity profiles at any position within the vasculature. This further permits us to model the profile theoretically and to adjust an equation whose parameters can be further used in the numerical simulation. Nevertheless, before performing numerical simulation of blood flow behavior in the ZF embryo, one should assess the efficacy of optical tweezing of circulating RBCs in developing blood vessels.

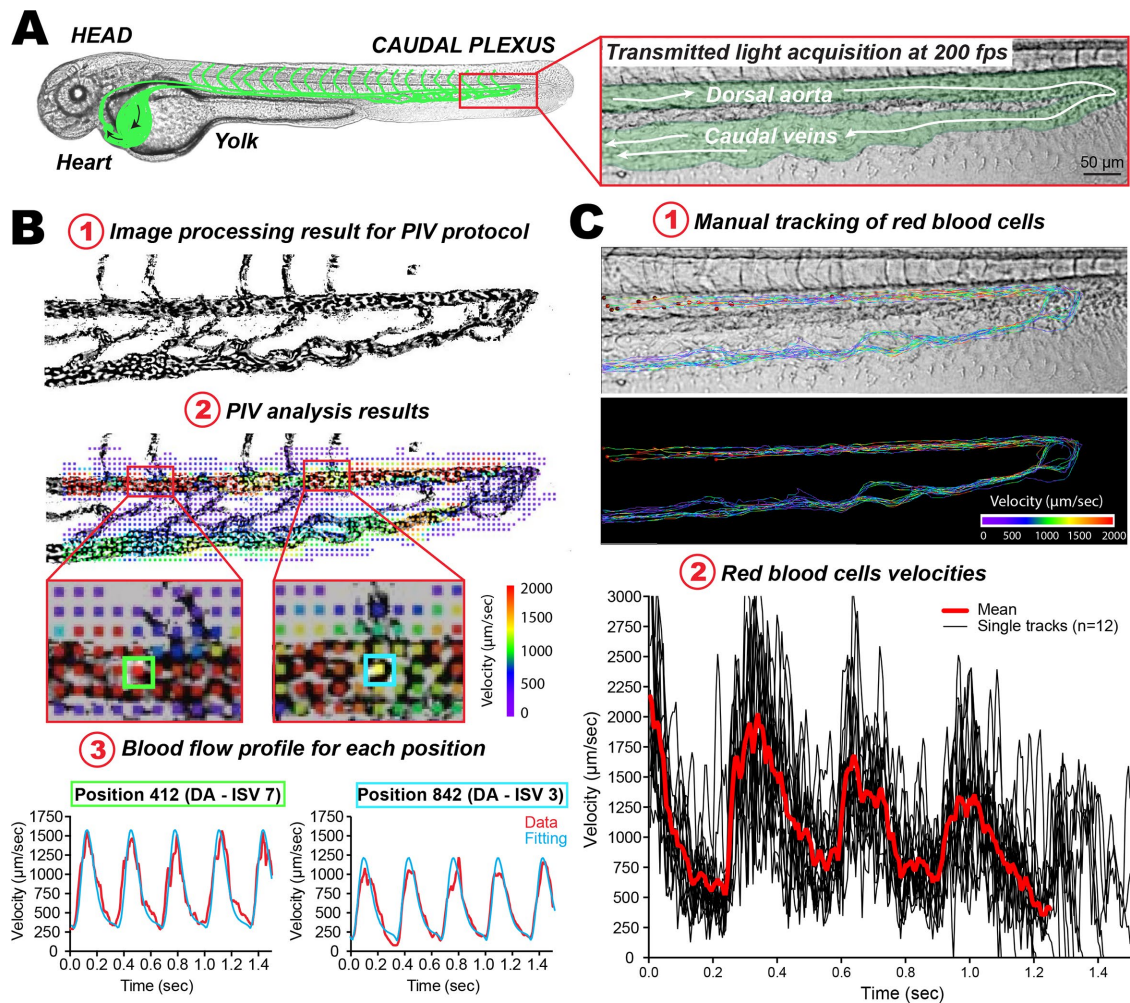


FIGURE 1: Fine measurements of blood flow velocities in the ZF embryo. (A) Experimental workflow: a representative image of a 48 hpf ZF embryo image is presented (the vasculature network is schematized in green), and a zoom of the caudal plexus region is presented in a separate box. (B) PIV analysis: 1) the images resulting from high-speed acquisition of the blood flow (200 fps) were processed such that high contrast is obtained for circulating RBCs. 2) The PIV analysis provides a color-coded velocity map over the entire image, in any region of interest. Flow profiles can thus be extracted at any given position. This further allows theoretical analysis of the flow values, which will be used in the simulation used for measuring the trap stiffness. 3) Here two positions, with distinct flow profiles and separated by roughly $250 \mu\text{m}$, are presented. Note the different flow profiles that can be observed and fitted. (C) Particle tracking analysis. Manual tracking of individual RBCs in perfused vessels can be performed. 1) Several tracks obtained over 12 RBCs are displayed. Tracks are color-coded according to their instantaneous velocity. Note the higher values and pulsatility obtained in the DA. 2) Instantaneous velocity frame after frame is plotted over a track spanning the entire caudal plexus, for 12 RBCs.

Optical trapping of RBCs, image analysis, and photodiode measurements

Although it is technically possible to trap RBCs (or other cells) anywhere in the ZF embryo (see Peralta *et al.*, 2013), we mostly performed optical tweezing in the caudal plexus. Here, in comparison to high-speed recording of the blood flow, a high magnification and numerical aperture objective is used to optically trap the RBCs in the flow (Figure 2A and Supplemental Movie S3). These trapped RBCs are mostly subjected to the dragging force of the blood flow and the restoring force of the OT (Jun *et al.*, 2014). We record the displacement of the RBCs within the optical trap on a quadrant photodiode at high frequency (more than 4 kHz) (Figure 2B). This temporal acquisition mirrors the cellular displacement from the trap center and is expressed in volts. Here we convert this displacement expressed in volts to displacement expressed in

micrometers by applying a conversion factor extracted from the two curves, allowing us to superimpose this curve to the displacement measured with the camera (Figure 2C). We further compute it as the power spectral density of the fluctuations (Figure 2B, black track), over which one can fit the OT behavior of a trapped cell in the absence of flow (as described in the Supplemental Methods). The parameters that are obtained allow us to extract a first approximation of the trap stiffness, which is $k = 4.7 \cdot 10^{-5} \text{ N/m}$. A similar temporal trapped RBC acquisition is simultaneously performed at 200 fps. The resulting kymograph shows the cellular displacement within the trap (Figure 2C) where accurate distances can be extracted (micrometers). From the cellular displacement in the trap and the measured stiffness, one can now convert the displacement track into an accurate force measurement (Figure 2D). When repeating the acquisition over the caudal plexus of the

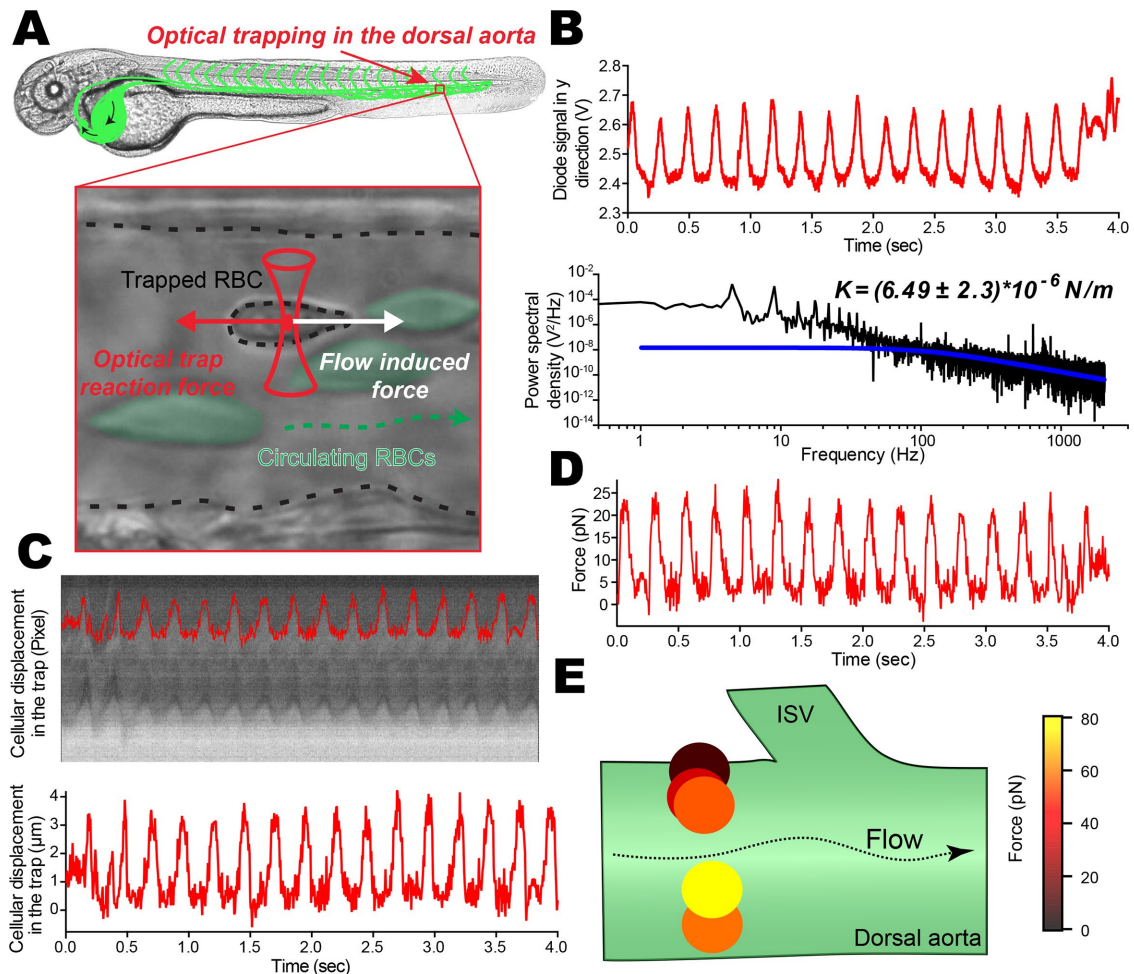


FIGURE 2: Optical trapping of circulating RBCs, image analysis and photodiode measurements. (A) Scheme of the experiment where the optical trap is located in the caudal plexus (DA) of the ZF embryo. The trapped RBC is subjected to the blood flow–driven dragging force as well as to the restoring force from the optical trap. (B) Thanks to the flow pulsatility occurring in arterial vessels, the time trace of the optically trapped RBC is followed on the quadrant diode. The time trace is further treated to access the power spectrum (black curve), revealing peaks of pulsatility as well as a corner frequency f_c around 250 Hz. This is highlighted with the theoretical curve for steady optical trapping experiments (blue curve). The cutoff frequency, obtained from a Lorentzian approximation, provides a first approximation of the trap stiffness, which is $\sim 4.7 \times 10^{-5} \text{ N/m}$. (C) A kymographic analysis of a single trapped RBC imaged at 200 fps is performed. Kymographs allow fine tracking of RBC displacement within the optical trap, thereby providing a real time track in micrometers. (D) A mirror force track over time is obtained and results from the use of the theoretical trap stiffness derived from the cutoff frequency (theoretical curve). (E) Any given position in the ZF vasculature can be probed, providing an accurate measure of hemodynamic forces. Here a few trapping RBCs in a cross-section of the DA permit appreciation of the behavior of a Poiseuille-type of flow.

2 dpf (days postfertilization) ZF embryo, we are now capable of drawing a hemodynamic force map (personal communication; Follain *et al.*, 2017). From the forces extracted with this method, it is also possible to elaborate the flow profile and thus to extract the shear stress one cell has to overcome once attached to the endothelium. In addition, one can now observe and highlight the Poiseuille flow profile of the developing dorsal aorta (DA) of a 2 dpf ZF embryo (Figure 2E). This allows quantifying both the velocity and the shear stress in close proximity to the endothelial walls. It is important to note at this stage that the calibration of OT was here performed in a blood vessel with pulsatile flow (DA). Such a parameter could greatly influence the measured trap stiffness, as well as the ways to measure it. However, our workflow now allows conducting numerical simulations that can be compared with the previous data.

Performing numerical simulations for accurate measurement of the trap stiffness

Before starting running simulations of *in vivo* experiments, one needs to verify and assess the robustness of the code (see the Supplemental Methods). We first performed simulations in the absence of external flow and tuned the trap stiffness from 10^{-5} to 10^{-4} N/m (Figure 3A). The model predicts that an increase in the trap stiffness should lead to a decrease in the fluctuations of the cell within the trap as well as an increase in the cutoff frequency. We next considered the presence of a pulsatile flow for which we imposed fixed velocity, frequency, and damping values while only tuning the trap stiffness again from 10^{-5} to 10^{-4} N/m . The flow parameters are the following: maximal velocity of $1300 \mu\text{m/s}$, frequency of 2.1 Hz, and damping $\tau = 0.8$ (the latter value corresponds to an average value obtained through the caudal plexus) (Figure 3, B and C). As expected, the trap

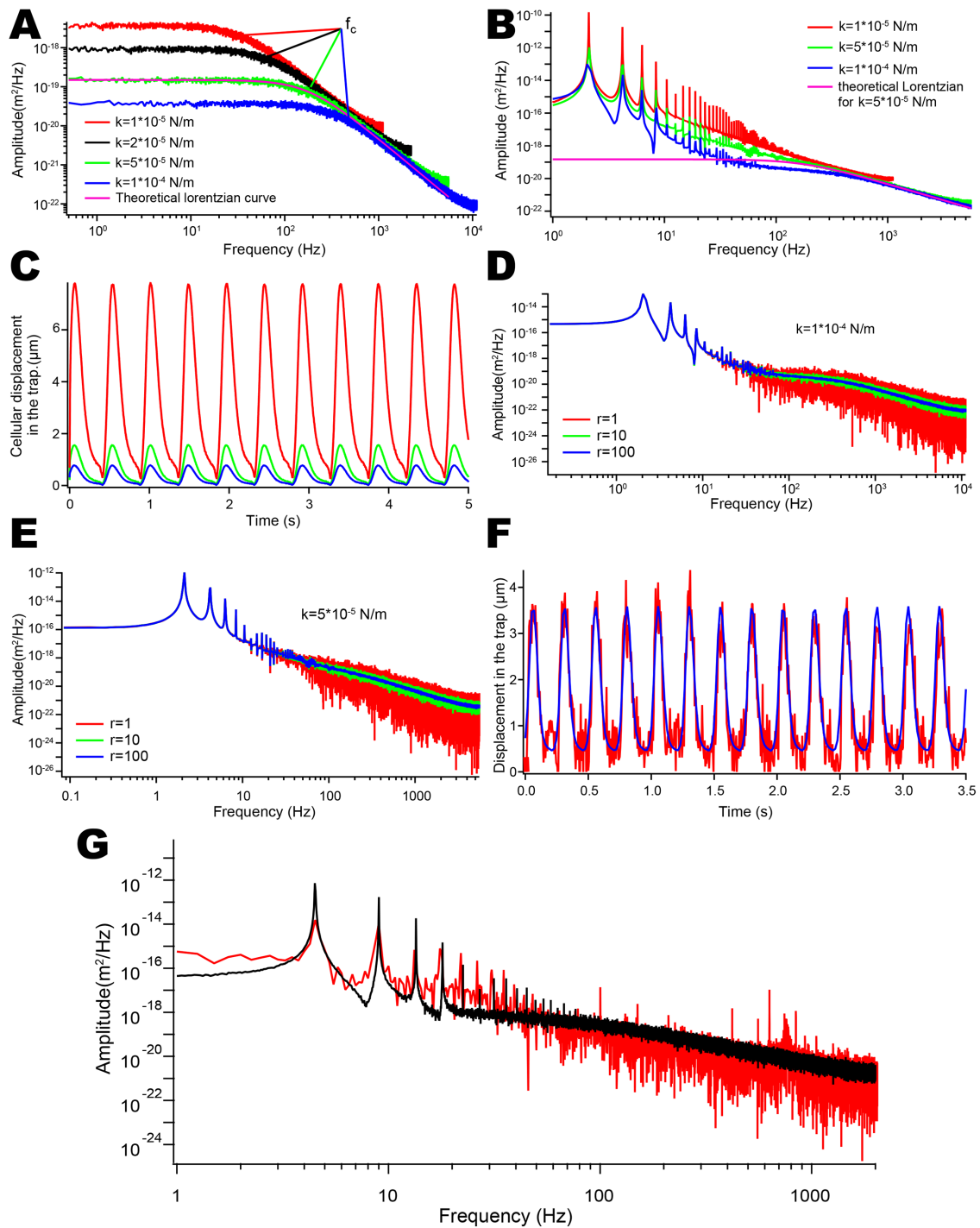


FIGURE 3: Numerical simulations. (A) Power spectrum of different tracks is represented graphically. No external pulsatile flow was applied, and the trap stiffness was modulated from 10^{-5} to 10^{-4} N/m to show that global fluctuations in the trap decreased when the stiffness was increased (ordinate at the origin) and that the cutoff frequency increases to higher frequency from 50 to 350 Hz. (B) Power spectral representations of different tracks resulting from same pulsatile flow. The trap stiffness is modulated from 10^{-5} to 10^{-4} N/m. The cutoff frequency increases to higher frequency when the stiffness increases as shown in A. The amplitude of the peaks at 2 Hz and its harmonics diminishes when the stiffness increases. (C) Movement of RBCs within the optical trap is tracked and plotted over time. Low trap stiffness allows trapped RBCs to reach $6 \mu\text{m}$ oscillations that are bigger than the cellular diameter and would lead to RBCs escaping the trap over time. (D) Three different power spectrum with constant velocity and physical parameters $k = 10^{-4}$ N/m, but with different spectral averaging from 1 to 100, are represented. While the signal-to-noise ratio is increasing as the square of the averages the cutoff frequency due to the trap stiffness was visible without averaging. (E) Three different power spectra with constant velocity and physical parameters $k = 5 \cdot 10^{-5}$ N/m, but with different averaging from 1 to 100. As in D, the signal-to-noise ratio is increasing as the square of the number of averages, nevertheless the cutoff frequency (around 150 Hz) is hardly visible even after 100 spectral averages. This is due to the overlap of the

stiffness affects the cutoff frequency in a manner similar to the those obtained in the absence of flow (Figure 3B). In addition, we observed and measured a significant decrease in the peak amplitude with increasing trap stiffness, confirming that the fluctuations of the cell within the trap are directly linked to the stiffness (Figure 3B). The simulation allows us to extract also the displacement of the RBCs over time, and these displacements clearly demonstrated the impact of the trap stiffness on the cellular movement (Figure 3C). More precisely, we observed a displacement of 7.7 μm within the trap when the stiffness was set to 10^{-5} N/m and a displacement of 770 nm when the stiffness was set to 10^{-4} N/m. A cellular displacement of 7.7 μm within the trap, which exceeds the radius of individual RBCs, will inevitably lead to the RBCs escaping from the trap. Such simulations confirm that stiffness of the trap impacts the cutoff frequency and linearly impacts the overall amplitude of fluctuations at low frequencies that are mainly driven by the amplitude of the flow. It is important to note at this stage that these simulations were run by averaging the spectral density over 100 runs. A major bottleneck of such an experiment is, however, the acquisition time, which should be as low as possible to exclude or prevent external perturbations such as drift of the sample/embryo or trapped RBCs that are being ejected from the trap by collision with other circulating RBCs. We therefore assessed the sensitivity of this method by modulating the number of temporal averages from 100 to 1 while keeping all the other parameters constant. We ran a first series of simulations at high trap stiffness ($k = 10^{-4}$ N/m) and observed that the trap cutoff frequency remains well defined when compared with the flow-driven frequency dependence (Figure 3D). We thus concluded that the number of acquisitions is irrelevant. Nevertheless, in a second experiment where the trap stiffness was set to 5×10^{-5} N/m (Figure 3E), we observed that such stiffness leads to a trap cutoff frequency that cannot be extracted from the flow-driven frequency dependence. Here a simulation averaging of 100 times is required to reach the trap cutoff frequency. In other words, probing forces at such parameters is incompatible with experimental recording that would require acquisition of ~ 100 s or more. For this reason, we rely now on the developed numerical code (Supplemental Methods) as well as on the fine flow mapping described previously (Figure 1). A combination of numerical code and fine flow mapping allows us to calibrate the optical trap from the experimental data by applying a fit to the obtained curves. First, we extract the experimental data from the signal obtained on the quadrant diode and transform them into a real displacement in micrometers (Figure 3F, red plot). We run the simulation with the flow parameters extracted from the previous PIV experiment and adjust the trap stiffness until the simulated displacement adjusts the experimental one (Figure 3F, blue plot). This theoretical curve gives a good approximation on the beating frequency and the endothelial damping. The values obtained from fine flow mapping (PIV + tracking; Figure 1) are fed into the numerical simulation as input parameters before running the fit and superimposing the power spectral density curves obtained experimentally (Figure 3G, red) and theoretically (Figure 3G, black). This example demonstrates the good accordance between velocity peaks induced by flow pulsatility and the appearance of the cutoff frequency around

250 Hz. Altogether this demonstrates that the calibration of the setup is achieved. This now gives access to fine blood flow force mapping at any position in the developing ZF embryo.

Blood flow tuning can be accurately assessed with optical tweezers in vivo

A proper calibration of the OT allows envisioning fine flow mapping in the ZF embryo. To demonstrate the power of such a method, we tuned the pacemaker activity using a previously described pharmacological treatment and measured its impact on flow profiles and applied forces. Lidocaine, a sodium channel blocker, has been shown to reduce significantly the pacemaker activity of 2 dpf ZF embryos (Cummins, 2007; Vermot *et al.*, 2009). Using high-speed imaging of heart beats, we observed that lidocaine reduced the pacemaker activity by 30–35% (data not shown; Follain *et al.*, 2017, personal communication) and impacted the flow velocity accordingly. These behaviors are in good agreement with previous work performed with lidocaine (Vermot *et al.*, 2009; Anton *et al.*, 2013; Heckel *et al.*, 2015). Optical tweezing of single RBCs was performed at two different positions in the caudal region of the DA of control and lidocaine-treated embryos (Figure 4, A and B). Before optical tweezing, flow profiles at each respective position were probed using high-speed imaging (200 fps) followed by PIV analysis. Flow mapping indicates a significant decrease in flow velocities imposed by lidocaine and the underlying reduction in pacemaker activity. Both flow pulsatility as well as velocity amplitude are reduced at both positions (Figure 4, C and D). We then trapped single RBCs at the two positions and tracked the cellular movement within the trap over time (Figure 4, E and F). Kymographic analysis revealed RBC oscillations within the trap, which can be plotted over time (Figure 4, G and H). The profiles that are obtained perfectly mirror the velocity profiles from the PIV analysis, with a marked decrease in both pulse frequency and flow amplitude. Nevertheless, as shown previously, the trap stiffness controls the amplitude of movement of RBCs within the trap. We thus adjusted the laser power such that RBCs would be held in the trap without escaping in the control experiments. We thus increased the laser power in the control condition compared with the lidocaine condition. We then extracted the trap stiffness from the power spectra adjusted using our previously described numerical model and plotted the force tracks that are associated with cellular displacements (Figure 4, I and J). Such an analysis allows us to accurately measure flow forces and, in that case, to probe the impact of a reduction in pacemaker activity on hemodynamic forces at high accuracy.

In conclusion, we have described here a fast and straightforward method to probe and measure hemodynamic forces in vivo. By combining flow profile dissection, power spectrum acquisition, and numerical analysis of the experimental data, we could extract the stiffness of the optical trap that is essential for correlating the trapping effect to the imposed force. The power of this method and analysis is that the numerical simulation provides a fast and reliable mean to assess trap stiffness and the underlying forces. As described previously (Zhong *et al.*, 2013) and detailed in the Supplemental Methods, one can neglect inertia. Indeed, the temporal

flow contribution in the power spectrum and the cutoff frequency due to trap stiffness making its distinction complicated. (F) Displacement of a single RBC within the optical trap is tracked and plotted over time. The blue curve represents the theoretical function of the flow pulses, which perfectly matches the experimental data. The obtained function is later used to model and fit the experimental power spectrum. (G) Experimental power spectrum is obtained from a trapped RBC. The black curve represents the fitting of the experimental red curve with the numerical model. Such fitting permits extraction with high accuracy the trap stiffness.

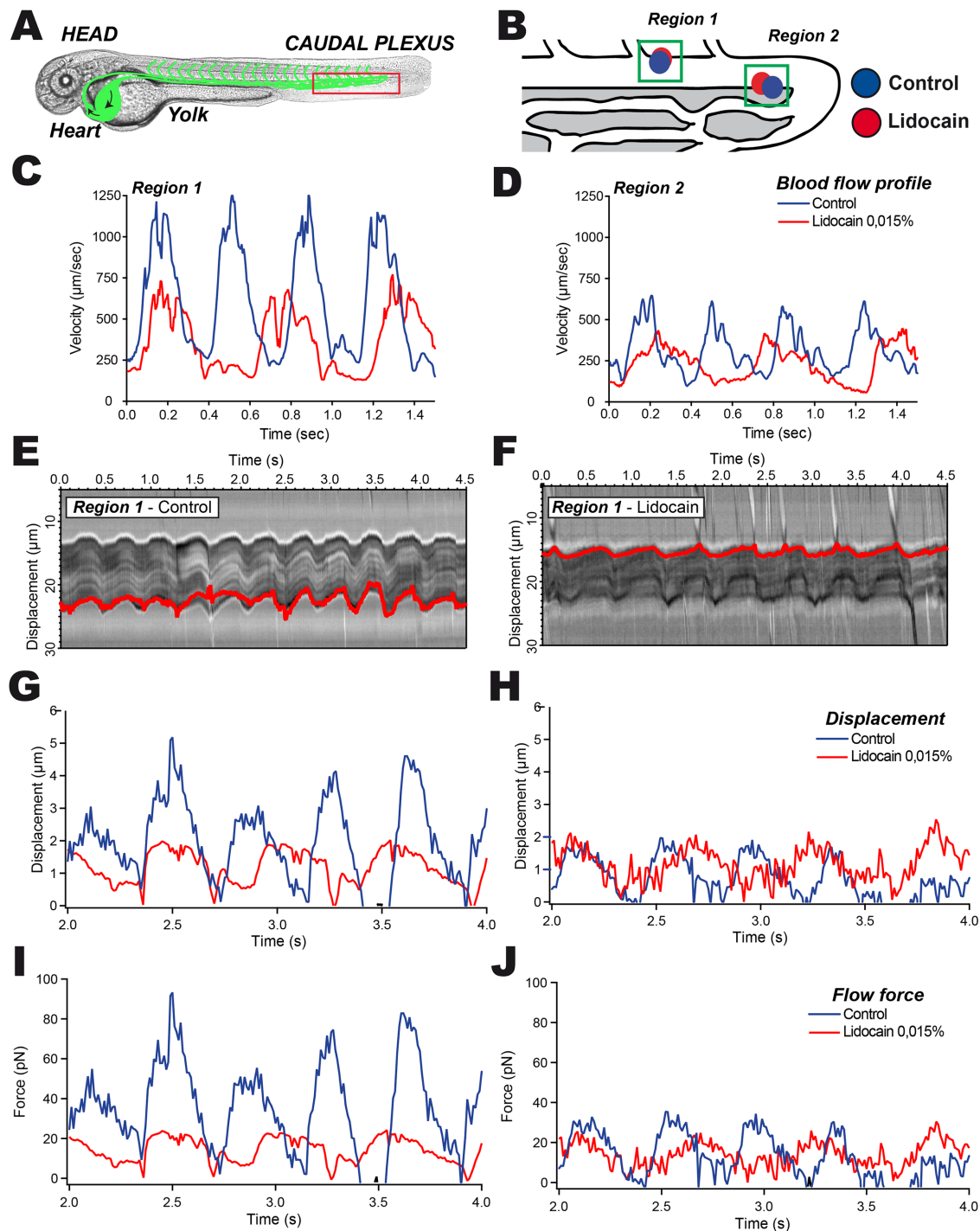


FIGURE 4: The impact of blood flow tuning on hemodynamic forces can be accurately measured using calibrated optical tweezing. (A) A representative image of the ZF embryo at 48 hpf is provided; the region of interest is highlighted in red. Blood flow tuning is achieved by pretreating the embryos with lidocaine (0.0015%). (B) Two positions within the caudal region of the DA are probed with OT. (C, D) PIV tracks are obtained from high-speed imaging and analysis of region 1 (C) and region 2 (D). (E, F) Kymographic analysis of the optically trapped RBC in region 1 in control (E) and lidocaine-treated (F) embryos. The displacement track is represented in red. (G, H) Displacement of the trapped RBC is measured and plotted in region 1 (G) and region 2 (H). (I, J) Force curves from region 1 (I) and 2 (J) are extracted from the displacement of RBCs within the calibrated optical trap.

resolution of imaging of the blood flow is limited and leads to two major forces: the restoring force exerted by the optical trap to the trapped object (i.e., a RBC) and the dragging force from the blood flow. These two forces have separated frequency responses. While the restoring force acts at high frequency (100–1000 Hz), the drag-

ging force, in the case of the ZF embryo, is closely linked to the heart beat frequency (around 2–3 Hz). In these conditions, previous work demonstrated analytically that two signals with frequency domains sufficiently separated could be solved in the Fourier domain as a sum of the two contributions (Seth Roberts *et al.*, 2007). In

that work they imposed oscillations at frequency far from the cutoff frequency to the trapped bead with an electrical field. From the collected oscillation, they plotted the power spectrum presenting a defined peak at the oscillation frequency. The amplitude of this peak due to its distance from the cutoff frequency was directly proportional to the number of charges created.

Our method suffers from two limitations. First, we consider RBCs as spherical objects from which the corresponding dragging force is derived. This consideration does not take into account RBC deformations. Second, we do not precisely measure the distance separating RBCs from the vessel wall and thus consider a constant viscosity instead of Faxen's law (Jun *et al.*, 2014). We therefore introduce underestimations in the resulting calibration. These underestimations represent an error on the force of ~20% close to the endothelial wall.

Altogether we have shown here that precise probing of hemodynamic forces using optical tweezing *in vivo* can be achieved. Such measurements, when applied to the understanding of hemodynamics in vascular morphogenesis (Sugden *et al.*, 2017), atherosclerosis (Namdee *et al.*, 2014), or thrombosis (Karachaliou *et al.*, 2015) events could provide unexpected insights into the contribution of fluid mechanics. When using the trapping function of OT, one can also redirect circulation of RBCs in the ZF embryo and unravel the importance of vascular architecture in driving its perfusion (Sugden *et al.*, 2017). Another important question that could be solved using this tool is the potential contribution of hemodynamics to intravascular arrest of immune or CTCs. Probing the shear stress in very close proximity to the vessel wall could help in understanding whether rolling of immune or tumor cells, usually attributed to selectin adhesion (Brunk and Hammer, 1997; Lawrence *et al.*, 1997; Sun *et al.*, 2015), can be tuned by hemodynamics. During their journey in the blood circulation, CTCs are subjected to shear forces and collisions with host cells. Only CTCs that overcome or exploit these forces will eventually arrest in vascular regions, preceding metastatic outgrowth. A major advantage provided by calibrated optical tweezing lies in the ability to probe hemodynamic forces precisely at the vessel wall. These regions cannot be reached with other classical flow mapping methods, although they are of utmost importance in the context of intravascular arrest of tumor or immune cells. Assessing, using calibrated optical tweezing, the impact of flow forces on such events, and many others, is thus within reach and could lead to very important observations in the near future.

MATERIALS AND METHODS

ZF handling and mounting for high-speed imaging

Tg(fli1a:eGFP) ZF (*Danio rerio*) embryos used in this study come from a Tübingen background. Embryos were maintained at 28°C in Danieau 0.3X medium (17.4 mM NaCl, 0.2 mM KCl, 0.1 mM MgSO₄, 0.2 mM Ca(NO₃)₂) buffered with HEPES 0.15 mM (pH = 7.6), supplemented with 200 μM of 1-phenyl-2-thiourea (Sigma-Aldrich) after 24 hpf. At 48 hpf, embryos were freed from their chorion and mount in an agarose drop (0.8%) deposited on a glass-bottomed dish (MatTek) compatible with high-resolution imaging. The embryos were positioned in the microscopic framework in order to overlap the DA longitudinal axis with the x-axis and the intersegmental vein (ISV) with the y-axis. For lidocaine treatment experiments, embryos were incubated in Danieau with 0.0015% lidocaine versus control vehicle (EtOH) for 2 h before mounting and imaging. Pacemaker activity of the heart was assessed using a USB 3.0 uEye IDS charge-coupled device (CCD) camera (IDEX) mounted on a DMIRE2 inverted microscope (Leica) using transmitted light. Heartbeats were acquired at 80 fps. Kymographic analysis was performed for extracting the beat frequency.

High-speed acquisition and PIV analysis

For the PIV analysis, high-speed recordings of the blood flow were performed using a Thorlabs DCC3240C Cmos camera at 200 fps mounted on the inverted microscope coupled with a UPLFLN 20X/0.4 objective (Olympus). The RBC positions at each frame were cross-correlated to the next frame using an adapted PIV protocol from ImageJ software available online (<https://sites.google.com/site/qingzongtseng/piv>). The individual displacements as well as the associated frame rate give then access to the individual velocity profiles of the blood cells in the bloodstream. These results were compared with results generated from manual particle tracking (ImageJ) sequences on the same movies. This allows to fine-tuning of the PIV parameters in order to access to the velocity distribution in the vasculature.

Optical trapping

A 1064 nm laser (Navigator 1064-7Y Spectra Physics) feeds the back aperture of the UPLFLNP 100X/1.3 objective (Olympus) to generate an optical trap; the objective is mounted on a thermostated inverted microscope. Trapping of RBCs was performed as described in Anton (2013) in a thermoregulated chamber ensuring the embryos to remain at 28°C. We acquired the displacement with the Thorlabs Cmos camera at 200 fps and simultaneously acquire the temporal signal on a quadrant photodiode at 20 kHz to calibrate the setup to reconstruct the power spectrum and thus allow the calibration of the trap.

Numerical simulation

A full and detailed description is provided in the Supplemental Methods. A general Langevin equation describing the Brownian evolution of a particle combined to an external flow reads

$$m\dot{\mathbf{x}}(t) = \xi[\dot{\mathbf{x}}(t) - u_e(t)] - K\mathbf{x}(t) + \Gamma(t)$$

In the present case, let us assume that the parameters are $\xi = 4.5 \cdot 10^{-8}$ N·s·m⁻¹ the Stokes friction coefficient of the cell, $K = 1 \cdot 10^{-4}$ N·m⁻¹ the OT spring stiffness, $u_e(t)$ the external pulsatile flow with a velocity of the order of a few millimeters per second, and $m = 2.1 \cdot 10^{-14}$ kg the mass of a blood cell of radius 1.5 μm and volume mass 1500 kg/m³ (in the absence of hydrodynamic corrections). $\Gamma(t)$ is the random noise, or Langevin force. This random force is supposed to be white, stationary, and Gaussian, with the standard time correlations.

$$\langle \Gamma(t)\Gamma(t') \rangle = 2kBT\xi\delta(t - t')$$

The overall process is Markovian. Considering now the effect of a periodic external force acting on the cell, one observes that three different regimes emerge, delimited by two characteristic frequencies $\omega_s/(2\pi)$ and $\omega_l/(2\pi)$. For $\xi\omega_s = K$, the friction force matches the tweezer restoring force, while for $\xi\omega_l = m\omega_l^2$ friction and inertia come out even. Straightforward numerical estimates lead to $\omega_s/(2\pi) = 350$ Hz and $\omega_l/(2\pi) = 340$ kHz.

At low frequencies ($f < 300$ Hz), the position of the cell in the optical trap follows closely the external drag force $\xi \cdot u_e$. At these frequencies, the trapped cell follows the regime dominated by the external flow and the optical trap stiffness. Inertia can be safely neglected in the range of frequencies $f < 10^4$ Hz for which experimental sampling is done. At frequencies between 300 and 10⁴ Hz, the position of the cell in the optical trap is dominated by thermal fluctuations and is represented on the power spectrum by a -2 power law. The frequency with which the cellular position switches from the dragging and trapping regime to the thermal fluctuations regime is called the cutoff frequency.

We therefore consider the overdamped, or Smoluchowsky, limit of the Langevin equation

$$-\xi(\dot{x}(t) - ue(t)) + Kx(t) + \Gamma(t) = 0$$

This equation represents the master equation used to run the numerical simulations.

ACKNOWLEDGMENTS

We thank all members of the Goetz lab for helpful discussions. We thank Julien Vermot for the original experiments in the ZF embryo. We are grateful to Pascal Kessler (Institut de Genetique et de Biologie Moleculaire et Cellulaire) for his help with the Imaris software. This work has been funded by labex NIE (S.H. and J.G.), Plan Cancer (OptoMetaTrap; J.G. and S.H.), and Centre National de la Recherche Scientifique (CNRS) IMAG'IN (S.H., J.G.) and by institutional funds from the Institut National de la Sante et de la Recherche Medicale (INSERM) and the University of Strasbourg. G.F. is supported by a PhD fellowship from La Ligue Contre le Cancer.

REFERENCES

- Amini H, Lee W, Di Carlo D (2014). Inertial microfluidic physics. *Lab Chip* 14, 2739.
- Anton H, Harlepp S, Ramspacher C, Wu D, Monduc F, Bhat S, Liebling M, Paoletti C, Charvin G, Freund JB, et al. (2013). Pulse propagation by a capacitive mechanism drives embryonic blood flow. *Development* 140, 4426–4434.
- Ashkin A, Dziedzic J (1987). Optical trapping and manipulation of viruses and bacteria. *Science* 235, 1517–1520.
- Azevedo S, Follain G, Patthabhiraman S, Harlepp S, Goetz JG (2015). Metastasis of circulating tumor cells: favorable soil or suitable biomechanics, or both? *Cell Adh Migr* 9, 345–356.
- Bambardekar K, Clément R, Blanc O, Chardès C, Lenne P-F (2015). Direct laser manipulation reveals the mechanics of cell contacts in vivo. *Proc Natl Acad Sci USA* 112, 1416–1421.
- Brunet T, Bouclet A, Ahmadi P, Mitrossilis D, Driquez B, Brunet A-C, Henry L, Serman F, Béalle G, Ménager C, et al. (2013). Evolutionary conservation of early mesoderm specification by mechanotransduction in Bilateria. *Nat Commun* 4, 2821.
- Brunk DK, Hamner DA (1997). Quantifying rolling adhesion with a cell-free assay: E-selectin and its carbohydrate ligands. *Biophys J* 72, 2820.
- Chang AC, Mekhdjian AH, Morimatsu M, Denisin AK, Pruitt BL, Dunn AR (2016). Single molecule force measurements in living cells reveal a minimally tensioned integrin state. *ACS Nano* 10, 10745–10752.
- Cummins TR (2007). Setting up for the block: the mechanism underlying lidocaine's use-dependent inhibition of sodium channels. *J Physiol* 582, 11.
- Desprat N, Supatto W, Pouille P-A, Beaurepaire E, Farge E (2008). Tissue deformation modulates twist expression to determine anterior midgut differentiation in *Drosophila* embryos. *Dev Cell* 15, 470–477.
- Follain G, Osmani N, Azevedo S, Allio G, Mercier L, Karreman M, Solecki G, Fekonja N, Hille C, Chabannes V, et al. (2017). Hemodynamic forces tune the arrest, adhesion and extravasation of circulating tumor cells. *bioRxiv* doi: 10.1101/183046.
- Freund JB, Goetz JG, Hill KL, Vermot J (2012). Fluid flows and forces in development: functions, features and biophysical principles. *Development* 139, 3063.
- Gao H, Metz J, Teanby NA, Ward AD, Botchway SW, Coles B, Pollard MR, Sparkes I (2016). In Vivo quantification of peroxisome tethering to chloroplasts in tobacco epidermal cells using optical tweezers. *Plant Physiol* 170, 263–272.
- Heckel E, Boselli F, Roth S, Krudewig A, Belting H-G, Charvin G, Vermot J (2015). Oscillatory flow modulates mechanosensitive *klf2a* expression through *trpv4* and *trpp2* during heart valve development. *Curr Biol* 25, 1354–1361.
- Hörner F, Meissner R, Polali S, Pfeiffer J, Betz T, Denz C, Raz E (2017). Holographic optical tweezers-based in vivo manipulations in zebrafish embryos. *J Biophoton*, doi:10.1002/jbio.201600226.
- Huang W, Anvari B, Torres JH, LeBaron RG, Athanasiou KA (2003). Temporal effects of cell adhesion on mechanical characteristics of the single chondrocyte. *J Orthop Res* 21, 88–95.
- Jain RK, Martin JD, Stylianopoulos T (2014). The role of mechanical forces in tumor growth and therapy. *Annu Rev Biomed Eng* 16, 321–346.
- Johansen PL, Fenaroli F, Evensen L, Griffiths G, Koster G (2016). Optical micromanipulation of nanoparticles and cells inside living zebrafish. *Nat Commun* 7, 10974.
- Jun Y, Tripathy SK, Narayana Reddy BRJ, Mattson-Hoss MK, Gross SP (2014). Calibration of optical tweezers for in vivo force measurements: how do different approaches compare. *Biophys J* 107, 1474–1484.
- Karachaliou N, Pilotto S, Briá E, Rosell R (2015). Platelets and their role in cancer evolution and immune system. *Transl Lung Cancer Res* 4, 713.
- Labernadie A, Kato T, Brugués A, Serra-Picamal X, Derzsi S, Arwert E, Weston A, González-Tarragó V, Elosegui-Artola A, Albertazzi L, et al. (2017). A mechanically active heterotypic E-cadherin/N-cadherin adhesion enables fibroblasts to drive cancer cell invasion. *Nat Cell Biol* 19, 224–237.
- Lawrence MB, Kansas GS, Kunkel EJ, Ley K (1997). Threshold levels of fluid shear promote leukocyte adhesion through selectins (CD62L, P, E). *J Cell Biol* 136, 717–727.
- Lopez-Quesada C, Fontaine A-S, Farré A, Joseph M, Selva J, Egea G, Ludevid MD, Martín-Badosa E, Montes-Usategui M (2014). Artificially-induced organelles are optimal targets for optical trapping experiments in living cells. *Biomed Opt Express* 5, 1993.
- Monachino E, Spenkelink LM, van Oijen AM (2017). Watching cellular machinery in action, one molecule at a time. *J Cell Biol* 216, 41–51.
- Namdeo K, Thompson AJ, Golinski A, Mocherla S, Bouis D, Eniola-Adefeso O (2014). In vivo evaluation of vascular-targeted spheroidal microparticles for imaging and drug delivery application in atherosclerosis. *Atherosclerosis* 237, 279–286.
- Peralta M, Steed E, Harlepp S, González-Rosa JM, Monduc F, Ariza-Cosano A, Cortés A, Rayón T, Gómez-Skarmeta J-L, Zapata A, et al. (2013). Heartbeat-driven pericardiac fluid forces contribute to epicardium morphogenesis. *Curr Biol* 23, 1726–1735.
- Petridou NI, Spiró Z, Heisenberg C-P (2017). Multiscale force sensing in development. *Nat Cell Biol* 19, 581–588.
- Provenzano PP, Hingorani SR (2013). Hyaluronan, fluid pressure, stromal resistance in pancreas cancer. *Br J Cancer* 108, 1–8.
- Reymond N, d'Água BB, Ridley AJ (2013). Crossing the endothelial barrier during metastasis. *Nat Rev Cancer* 13, 858–870.
- Seth Roberts G, Wood TA, Frith WJ, Bartlett P (2007). Direct measurement of the effective charge in nonpolar suspensions by optical tracking of single particles. *J Chem Phys* 126, 194503.
- Staunton JR, Blehm B, Devine A, Tanner K (2017). In situ calibration of position detection in an optical trap for active microrheology in viscous materials. *Optics Express* 25, 1746.
- Sugden WW, Meissner R, Aegerter-Wilmsen T, Tsaryk R, Leonard EV, Bussmann J, Hamm MJ, Herzog W, Jin Y, Jakobsson L, et al. (2017). Endoglin controls blood vessel diameter through endothelial cell shape changes in response to haemodynamic cues. *Nat Cell Biol* 19, 653–665.
- Sugimura K, Lenne P-F, Graner F (2016). Measuring forces and stresses in situ in living tissues. *Development* 143, 186–196.
- Sun G, Liu K, Wang X, Liu X, He Q, Hsiao C-D (2015). Identification and expression analysis of zebrafish (*Danio rerio*) E-selectin during embryonic development. *Molecules* 20, 18539–18550.
- Vermot J, Forouhar AS, Liebling M, Wu D, Plummer D, Gharib M, Fraser SE (2009). Reversing blood flows act through *klf2a* to ensure normal valvulogenesis in the developing heart. *PLoS Biol* 7, e1000246.
- Wirtz D, Konstantopoulos K, Searson PC (2011). The physics of cancer: the role of physical interactions and mechanical forces in metastasis. *Nat Rev Cancer* 11, 512–522.
- Zhong M-C, Wei X-B, Zhou J-H, Wang Z-Q, Li Y-M (2013). Trapping red blood cells in living animals using optical tweezers. *Nat Commun* 4, 1768.